Carbon–Silicon Schottky Barrier Diodes

*Chanyoung Yim, Niall McEvoy, Ehsan Rezvani, Shishir Kumar, and Georg S. Duesberg**

Schottky barrier diodes (SBDs) consisting of a metal-semiconductor contact are one of the simplest devices in modern semiconductor technology. In spite of the fact that Schottky diodes have a simple structure, they are the basis of a large number of compound semiconductor devices such as integrated circuits, high-frequency units, photodiodes, and power diodes.[1,2] In particular in mobile communication and power management there is an increasing demand for high-speed and high-performance diodes. Novel materials such as III–V semiconductors and SiC SBDs can provide higher performance than traditional silicon devices; however the cost of substrates is very high. Thus, novel materials meeting high performance at low cost have great commercial opportunities.

In general, the performance of the SBDs can be described with the ideality factor which is a value of how closely the diode follows the ideal diode behavior on a logarithmic scale. Typical diodes have ideality factors between 1 and 2, and in commercial products values between 1.05 and 1.2 are generally used. In addition, the stability of the interface between metal and semiconductor is one of the most critical conditions in diode performance. It is important to choose a proper material depending on the current density of the diode device. Since the discovery of carbon nanotubes and graphene, their use for nano-electronics devices has been widely proposed;[3–9] however questions over their integration into devices remain. The use of graphene in a SBD has been shown principally by Chen et al.; however a lot of improvements in fabrication and performance are needed before applications can be considered.[10] On the other hand, glassy and pyrolytic carbon can be fabricated at low cost with reliable results. Pyrolytic carbon (PyC), a disordered nanocrystalline graphitic material which can be formed through gas phase dehydrogenation (or pyrolysis) of hydrocarbons, exhibits good thermal and electrical conductivity as well as high durability.[11] Lately, PyC has been suggested for microelectronics applications including vias and wires, gate electrodes, and as a liner for trench capacitors in dynamic random access memory devices (DRAMs).[12–14] As for electrochemical applications, bulk glassy carbon has been commercially used as an electrode material for over half a century due to its excellent thermal and electrical stability, large potential window, and low background noise.[15] Its good electrical conductivity lends to applications in microbatteries where micromachined structures of glassy carbon are used as electrodes.[16] Glassy carbon films from pyrolyzed photoresist films (PPF) have tunable conductivity via pyrolysis temperatures and have been investigated as transparent conductors.[17–19] Despite these beneficial properties no detailed investigation into the use of these carbon materials in SBDs has been reported.

In this work, carbon films were used on a silicon (Si) wafer instead of a metal layer in order to fabricate SBD devices. The diodes were fabricated by a simple spin-coating and annealing of photoresist films or by the chemical vapor deposition of pyrolytic carbon onto n-type silicon (n-Si) wafers. After patterning and etching with a metal hardmask the current–voltage characteristics of SBDs were recorded. We extracted the parameters that control the device performance, such as barrier height (ϕ_B), ideality factor (n), and series resistance (R_S) from the current–voltage characteristics at room temperature.

The schematic and an optical microscopy image of the diodes are depicted in **Figure 1**. The area of the interface is approximately 3.1×10^{-2} cm^2 without the usage of any guard ring to prevent leakage currents at the device perimeter. The high-resolution transmission electron microscopy (HRTEM) analysis of the layers shows an amorphous structure typical for PPFs (**Figure 2**a). The gas phase deposited PyC film shows a slight laminar structure parallel to the underlying substrate (Figure 2b). The Raman spectra of PPF and PyC are nearly identical and typical for highly disordered sp^2 carbon materials (Figure 2c). PPF has a slightly larger D/G ratio than PyC, suggesting a higher degree of disorder which is in agreement with our TEM observations. The thickness of the carbon layer is ~78–80 nm for the PPF layer and ~62–65 nm for the PyC layer taken from cross-sectional TEM images. This is in agreement with the appearance of the a Si peak in the PyC Raman spectrum below 1000 cm^{-1} which stems from the substrate, indicating that here the PyC film is slightly thinner than the PPF film, and therefore still optically transparent.[11,19] The resistivity values, deduced from four-point measurements on

C. Yim, E. Rezvani, S. Kumar, Prof. G. S. Duesberg
School of Chemistry
Trinity College Dublin
Dublin 2, Dublin, Ireland
E-mail: duesberg@tcd.ie
C. Yim, Dr. N. McEvoy, E. Rezvani, S. Kumar, Prof. G. S. Duesberg
Centre for Research on Adaptive Nanostructures and Nanodevices (CRANN)
Trinity College Dublin
Dublin 2, Dublin, Ireland

DOI: 10.1002/smll.201101996

small NANO MICRO

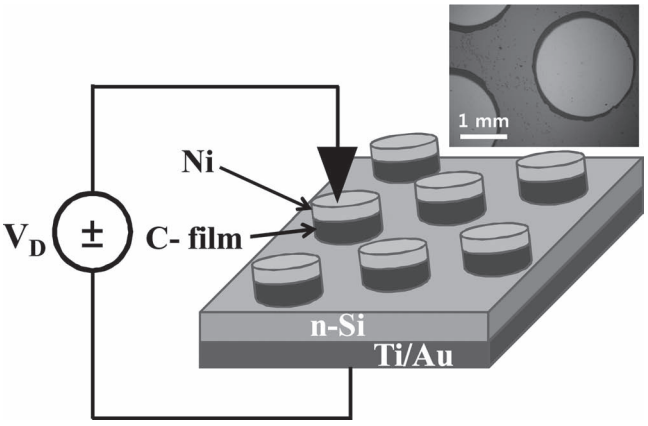

Figure 1. Schematic and optical microscope image (top view) of the carbon/n-Si Schottky barrier diode.

insulating substrates, are 4.0×10^{-5} and 2.5×10^{-5} Ω m for the PPF and PyC films, respectively. These similarities are remarkable as the two materials are related to glassy (PPF) and nanocrystalline (PyC) carbon structures. The interface between a PPF/PyC film and the Si substrate is shown in Figure 2a and b. No obvious interface layer between carbon and Si is visible, implying a direct linking of the crystalline Si to the carbon layers. However, at the interface between PyC and Si, the contrast is slightly lighter, which may indicate the presents of interfacial oxides. Thus both methods yield a very clean and atomically thin interface region assuming direct Si–C bonds, even though the complete absence of SiO_2 from residual H_2O or O_2 cannot be ruled out from HRTEM studies.

The current–voltage (*I–V*) characteristics of carbon films on n-Si substrates were measured in the voltage range of ±4 V. The forward and reverse biased semi-log *I–V* characteristics of the PPF/n-Si and PyC/n-Si at room temperature are shown in **Figure 3**. In forward-bias, the nickel metal dot electrode was positively biased, and the backside Ti/Au electrode was negatively biased. *I–V* characteristics of the carbon/n-Si SBD show rectifying behavior which is limited by the magnitude of the energy barrier at the junction interface.[20] It is clearly demonstrated that while the current becomes saturated under the reverse bias, the current increases exponentially under the forward bias. Forward bias *I–V* characteristics are linear at low voltage in the semi-log plot, but in the high-voltage range it deviates from the linear behavior mainly due to the presence of the effect of series resistance (R_S) which is associated with the bulk material in the semiconductor and the ohmic backside contact.

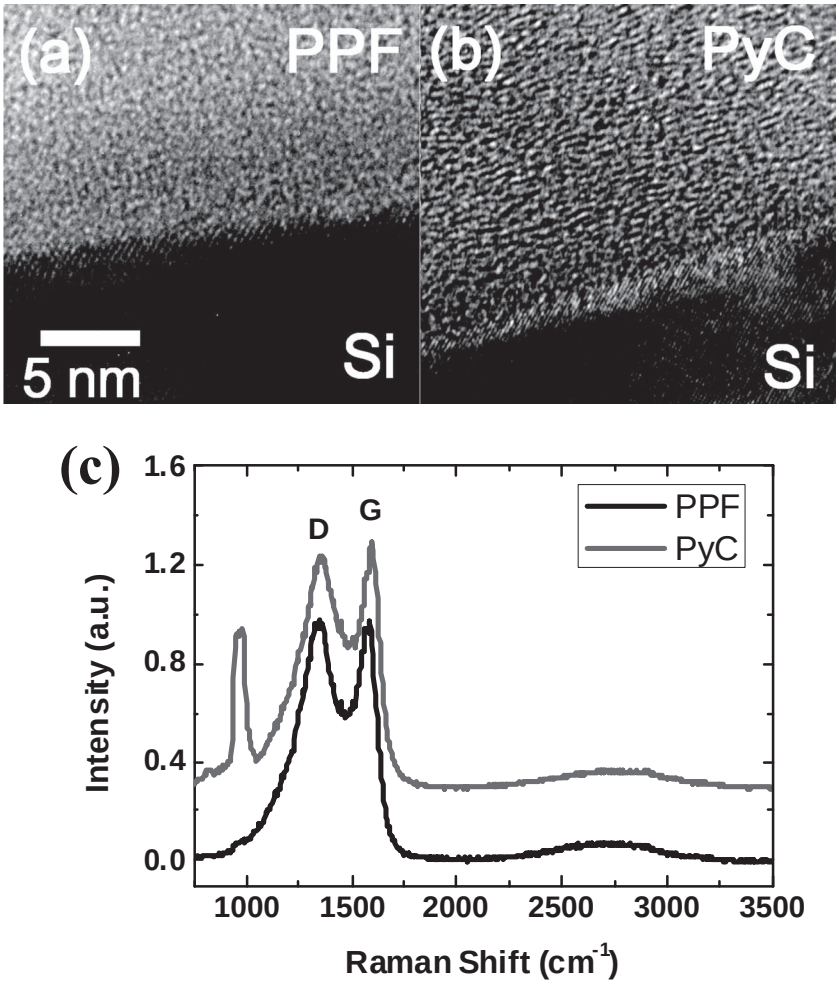

Figure 2. TEM images of a) the PPF–Si interface region and b) the PyC–Si interface region. c) Raman spectra of PPF and PyC.

It is well known that the characteristics of the metal–semiconductor junction have a dominant influence on the performance of SBDs.[21,22] Therefore, the understanding of the electrical properties of the interface between metal and semiconductor is important for device applications. The current transport in metal–semiconductor contacts is explained with emission of electrons from the semiconductor over the potential barrier into the metal as the dominant process in SBD with moderately doped semiconductors, so the transport for the common high-mobility semiconductors such as silicon and gallium arsenide can be described by this thermionic-emission theory.[21] Therefore in the ideal case the electrical characteristics of SBDs are expected to obey the thermionic-emission theory, but in practice there are second-order effects so that the diode does not follow the simple diode equation. There are several possible reasons of errors that cause deviation of the ideal behavior of SBDs including the series resistance, the insulating layer between metal and semiconductor, and the interface states.[23,24] The ideality factor of a diode is a value of how closely the diode follows the ideal diode behavior on a logarithmic scale, and

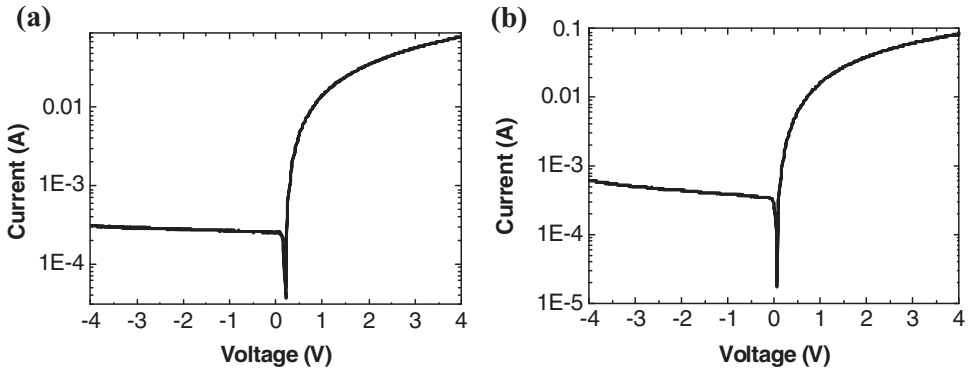

Figure 3. Semi-log *I–V* curve of carbon/n-Si Schottky diode a) for PPF/n-Si diode and b) for PyC/n-Si diode.

this value is close to unity in the device where the current transport is determined by thermionic emission process.

It is assumed that the current in the Schottky contact is due to thermionic emission. According to thermionic emission theory, the relationship between the current I and the voltage drop across the junction V_D is given by the following equation:[22]

$$I = I_S\left(\exp\frac{qV_D}{nkT} - 1\right) \quad (1)$$

where I_S is the reverse saturation current and can be expressed as

$$I_S = AA^{**}T^2\exp\left(\frac{-q\phi_B}{kT}\right) \quad (2)$$

where q is the elementary charge, T is temperature in Kelvin, k is the Boltzmann constant, n is the ideality factor, A is the effective diode area, A^{**} is the effective Richardson constant, and ϕ_B is the effective barrier height at zero bias. Since the effect of series resistance R_S on a diode is usually modeled with a series combination of a diode and a resistor with resistance R through which the current I flows, the voltage across the diode can be expressed in terms of the total voltage drop V across the series combination of the diode and the resistor. Thus, $V_D = V - IR_S$, and for $V_D > 3kT/q$, Equation 1 becomes

$$I = I_S\exp[q(V - IR_S)/nkT] \quad (3)$$

Taking the effect of series resistance into account, the electrical parameters of the diode device cannot be extracted from semi-log *I–V* plots directly. Thus, the electrical parameters of the diodes were calculated by two different methods.

The first one is based on the method developed by S. K. Cheung and N. W. Cheung.[25] Equation 3 can be rewritten in terms of current I. Thus,

$$V = IR_S + n\phi_B + \left(\frac{nkT}{q}\right)\ln\left(\frac{I}{AA^{**}T^2}\right) \quad (4)$$

When the Equation 4 is differentiated with respect to the current I, we obtain

$$\frac{d(V)}{d(\ln I)} = IR_S + \frac{nkT}{q} \quad (5)$$

The value of R_S and $n(kT/q)$ are obtained from the slope and y-axis intercept of the graph $d(V)/d(\ln I)$ versus I. Also, from Equation 4, $H(I)$ can be defined as

$$H(I) = V - \left(\frac{nkT}{q}\right)\ln\left(\frac{I}{AA^{**}T^2}\right) \quad (6)$$

$$H(I) = IR_S + n\phi_B \quad (7)$$

Using the value of n determined from Equation 5 and the data from Equation 6, the plot of $H(I)$ versus I from Equation 7 gives a straight line with y-axis intercept equal to $n\phi_B$. In addition, the slope of this plot gives the value of series resistance by which the consistency of R_S from Equation 5 can be checked.

The graphs of $dV/d(\ln I)$ versus I and $H(I)$ versus I for the PPF/n-Si and PyC/n-Si SBD devices are shown in **Figure 4**a and b. On the PPF/n-Si SBD device, the determined values of series resistance from the plots of $dV/d(\ln I)$ versus I and $H(I)$ versus I are 44.83 and 44.78 Ω, respectively, which are in excellent agreement. The values of the ideality factor and the barrier height were found to be 1.28 and 0.69 eV, respectively. In the case of the PyC/n-Si SBD, the values of R_S from the plots of $dV/d(\ln I)$ versus I and $H(I)$ versus I are 42.10 and 42.18 Ω with the values of $n = 1.44$ and $\phi_B = 0.60$ eV.

Furthermore, the electrical parameters of the diode were also investigated using Norde's method.[26] The function $F(V)$ is defined as

$$F(V) = \frac{V}{2} - \left(\frac{kT}{q}\right)\ln\left[\frac{I(V)}{AA^{**}T^2}\right] \quad (8)$$

where $I(V)$ is the current obtained from the *I–V* curve of the diode and other parameters are described above. Once the minimum of the $F(V)$ versus V plot is determined, the Schottky barrier height is obtained using

$$\phi_B = F(V_0) + \frac{V_0}{2} - \frac{kT}{q} \quad (9)$$

where $F(V_0)$ is the minimum point of $F(V)$, and V_0 is the corresponding voltage.[27,28] Figure 4c and d show the $F(V)$ versus V plots for the PPF/n-Si and PyC/n-Si SBD devices. The values of ϕ_B for the PPF/n-Si and PyC/n-Si SBD devices

small NANO MICRO

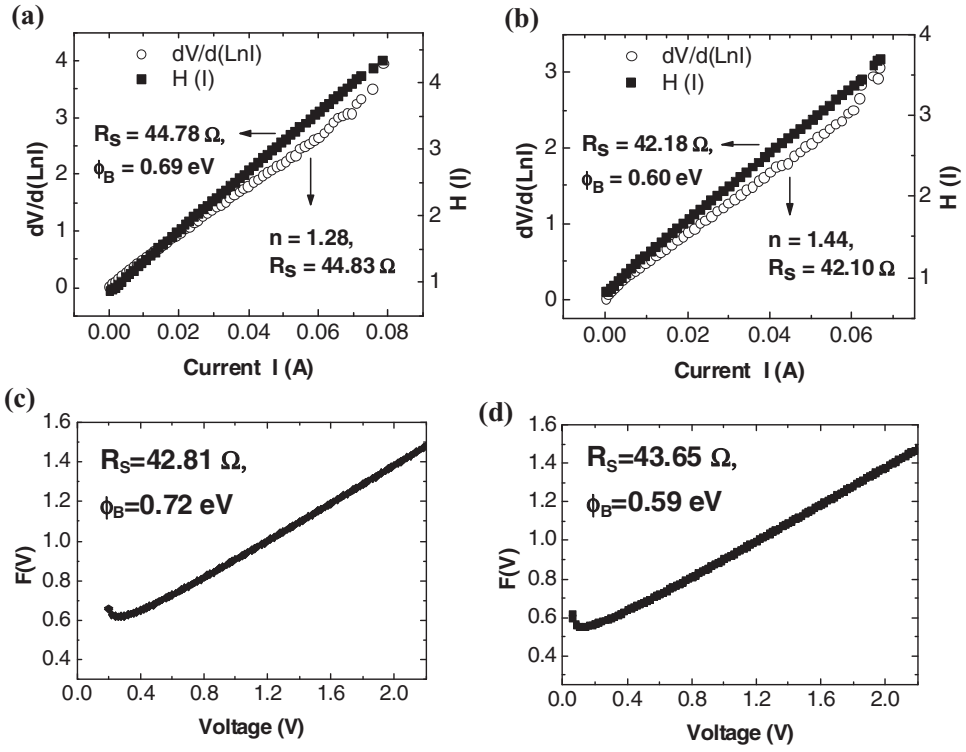

Figure 4. Plots of d*V*/d(ln*I*) versus *I* and *H*(*I*) versus *I* for a) PPF/n-Si diode and b) PyC/n-Si diode. Plots of *F*(*V*) versus *V* for c) PPF/n-Si diode and d) PyC/n-Si diode.

are 0.72 eV and 0.59 eV, respectively. The values of the series resistance were determined by using the following equation:

$$R_S = \frac{kT}{q\,I_0} \tag{10}$$

where I_0 is the current corresponding to the minimum V_0.[29] Using Equation 10, we found R_S = 42.81 Ω for the PPF/n-Si SBD device and R_S = 43.65 Ω for the PyC/n-Si SBD device. It can be seen from **Table 1** that the values of Schottky diode parameters obtained from each method are in good agreement. In addition, the result from *I*–*V* measurements taken on six different carbon/n-Si SBD devices shows the average values of each diode parameter for these devices are n = 1.29, ϕ_B = 0.71 eV, R_S = 52.25 Ω for the PPF/n-Si SBD devices, and n = 1.44, ϕ_B = 0.56 eV, R_S = 49.96 Ω for the PyC/n-Si SBD devices.

This is without any further optimization a remarkable result. Compared with recent result of graphene–Si SBDs,[10] it shows much better performance with a fourfold smaller of ideality factor which at room temperature. The reason for the better performance of our carbon–silicon SBDs in comparison with graphene–Si SBDs can be explained in two ways. The first reason is a formation of direct contact between the crystalline silicon and the disordered carbon in our devices, whereas in the case of graphene–Si SBDs the influence of the graphene–Si interface on the current transport would be more dominant as graphene gets transferred mechanically. The second reason is that our carbon material (PPF and PyC) shows nearly metallic characteristics, which forms invulnerable Schottky barrier with n-type silicon, while graphene is semi-metallic. Although our devices and the graphene–Si SBD devices use carbon material instead of metal for SBDs, the difference of material characteristics between two types of carbon material cause the difference in thermionic emission charge transport process. Moreover, our diodes have a very simple integration scheme and both carbon depositions are very cost-effective processes. A more advanced integration scheme, including guard rings to avoid edge leakage, complete removal of any possible Si oxidation at the interface and a reduction of the series resistance could give even better performance. The SB height also could be optimized by either changing the doping level of the Si substrate or by modifying the carbon layer. Further benefits and application fields have to be investigated in detail, but high stability allowing for high driving currents can be expected, due to the absence of metal silicide formation and the persistency towards electromigration in the carbon layers. The stability of our diodes is expected to be extremely high, as the fabrication process temperature is 1000 and 950 °C for PPF and PyC, respectively.

In this study, we have fabricated a new type of Schottky barrier diode between carbon and n-type silicon substrates.

Table 1. The parameter values of the carbon/n-Si Schottky barrier diodes obtained from *I*–*V* characteristics at room temperature.

	d*V*/d(ln*I*) versus *I*		*H*(*I*) versus *I*		*F*(*V*)	
Device	n	R_S [Ω]	ϕ_B [eV]	R_S [Ω]	ϕ_B [eV]	R_S [Ω]
PPF/n-Si	1.28	44.83	0.69	44.78	0.72	42.81
PyC/n-Si	1.44	42.10	0.60	42.18	0.59	43.65

The electrical parameters such as ideality factor, series resistance, and barrier height, were extracted using two different methods. The ideality factor values of these two different SBD devices were found to be $n = 1.28$ for the PPF/n-Si diode and $n = 1.44$ for the PyC/n-Si diode. This is in the reach of commercial diode devices, where the ideality factor is between 1.05 and 1.2, as it is expected that optimization would lead to higher device performance.

Experimental Section

Sample Preparation: n-Type silicon (n-Si) wafers with a dopant concentration of 5×10^{14} cm^{-3} and (100) orientation, were used as substrates. These were placed in 3.3% diluted hydrofluoric acid (HF) for 1 min to remove the native oxide from the Si surface. Two different types of carbon films were deposited. Firstly, AZ nLOF 2070, which is a negative-tone photoresist, was spin-coated at speeds of 5000 rpm for 45 s and annealed in a furnace at 1000 °C for 1 h as described previously.[19] Upon pyrolysis, the resist forms a thin conductive carbon layer known as pyrolyzed photoresist films (PPF). Secondly, the PyC layer was deposited on the n-type Si wafer through the process of chemical vapor deposition (CVD). PyC films were grown in a Gero quartz tube furnace (700 × 90 mm) using acetylene (C_2H_2) as the hydrocarbon feedstock at a flow rate of 180 sccm. A temperature of 950 °C was used with a pressure of 20 Torr and a dwell time of 5 min.

A shadow mask was used to deposit metal dot with radius of 1 mm arrays of nickel with 50 nm thickness. Each nickel/carbon/silicon dot operated as a separate diode. The carbon film between the metal dot patterns was removed with oxygen plasma etching using the nickel dots as a hardmask. Before making the backside metal contact on the silicon substrate, oxygen plasma etching was performed in order to get rid of the carbon residue on the backside of the wafer, followed by etching in 3.3% diluted hydrofluoric acid (HF) for 1 min for the removal of the native oxide and other contamination. For the backside metal contact, 20 nm of titanium and 40 nm of gold were deposited in situ with a sputter coating. All metal layers were deposited using Gatan Model 682 PECS.

Characterization: HRTEM studies were performed on cross sections of PPF and PyC on Si prepared in a Zeiss Auriga Focused Ion Beam (FIB) with a Cobra ion column. A reactive gas injection system was used for reactive ion etching and deposition of a Pt capping layer. These cross-sections were imaged at 300 kV using an FEI Titan 80-300 (S) TEM equipped with a S-TWIN objective lens and a high-brightness (X-FEG) Schottky field-emission gun with a monochromator. Raman spectra were taken with a Witec Alpha 300 R with an excitation wavelength of 532 nm. The electrical measurement for the current–voltage characteristics was carried out on a probe station connected to a Keithley 2400 source meter unit at room temperature.

Supporting Information

Supporting Information is available from the Wiley Online Library or from the author.

Acknowledgements

This work was supported by the SFI under Contract No. 08/CE/I1432 and 08/CE/I1432s1. GSD acknowledges SFI for PI_10/IN.1/I3030 grant, CY and SK acknowledge the Embark Initiative for IRCSET scholarships. We acknowledge the support of the Advanced Microscopy Lab.

[1] R. L. Vanmeirhaeghe, W. H. Laflere, F. Cardon, *J. Appl. Phys.* **1994**, *76*, 403.
[2] A. I. Prokopyev, S. A. Mesheryakov, *Measurement* **2003**, *33*, 135.
[3] M. Terrones, *Int. Mater. Rev.* **2004**, *49*, 325.
[4] M. P. Anantram, F. Leonard, *Rep. Prog. Phys.* **2006**, *69*, 507.
[5] K. Balasubramanian, M. Burghard, *J. Mater. Chem.* **2008**, *18*, 3071.
[6] Z. Liu, L. Jiao, Y. Yao, X. Xian, J. Zhang, *Adv. Mater.* **2010**, *22*, 2285.
[7] A. P. Graham, G. S. Duesberg, R. V. Seidel, M. Liebau, E. Unger, W. Pamler, F. Kreupl, W. Hoenlein, *Small* **2005**, *1*, 382.
[8] A. Nourbakhsh, M. Cantoro, A. Hadipour, T. Vosch, M. H. van der Veen, M. M. Heyns, B. F. Sels, S. De Gendt, *Appl. Phys. Lett.* **2010**, 97.
[9] S. Tongay, T. Schumann, X. Miao, B. R. Appleton, A. F. Hebard, *Carbon* **2011**, *49*, 2033.
[10] C.-C. Chen, M. Aykol, C.-C. Chang, A. F. J. Levi, S. B. Cronin, *Nano Lett.* **2011**, *11*, 1863.
[11] N. McEvoy, N. Peltekis, S. Kumar, E. Rezvani, H. Nolan, G. P. Keeley, W. J. Blau, G. S. Duesberg, *Carbon* **2012**, *50*, 1216.
[12] A. P. Graham, G. Schindler, G. S. Duesberg, T. Lutz, W. Weber, *J. Appl. Phys.* **2010**, 107.
[13] G. Raghavan, J. L. Hoyt, J. F. Gibbons, *Jpn. J. Appl. Phys., Part 1* **1993**, *32*, 380.
[14] G. Aichmayr, A. Avellán, G. S. Duesberg, F. Kreupl, S. Kudelka, M. Liebau, A. Orth, A. Sänger, J. Schumann, O. Storbeck, *Symposium on VLSI Technol. Digest of Tech. Pap.* **2007**, *10B*, 186.
[15] R. L. McCreery, *Chem. Rev.* **2008**, *108*, 2646.
[16] M. P. Manoharan, H. Lee, R. Rajagopalan, H. C. Foley, M. A. Haque, *Nanoscale Res. Lett.* **2010**, *5*, 14.
[17] J. Kim, X. Song, K. Kinoshita, M. Madou, B. White, *J. Electrochem. Soc.* **1998**, *145*, 2314.
[18] R. Kostecki, B. Schnyder, D. Alliata, X. Song, K. Kinoshita, R. Kotz, *Thin Solid Films* **2001**, *396*, 36.
[19] M. Schreiber, T. Lutz, G. P. Keeley, S. Kumar, M. Boese, S. Krishnamurthy, G. S. Duesberg, *Appl. Surf. Sci.* **2010**, *256*, 6186.
[20] T. Kilicoglu, *Thin Solid Films* **2008**, *516*, 967.
[21] S. M. Sze, *Physics of Semiconductor Devices*, 3rded., Wiley, New York **2007**, p. 134.
[22] E. H. Rhoderick, R. H. Williams, *Metal–Semiconductor Contacts*, Clarendon Press, Oxford **1988**.
[23] R. T. Tung, *Phys. Rev. B* **2001**, 64.
[24] A. Keffous, M. Siad, S. Mamma, Y. Belkacem, C. L. Chaouch, H. Menari, A. Dahmani, W. Chergui, *Appl. Surf. Sci.* **2003**, *218*, 336.
[25] S. K. Cheung, N. W. Cheung, *Appl. Phys. Lett.* **1986**, *49*, 85.
[26] H. Norde, *J. Appl. Phys.* **1979**, *50*, 5052.
[27] W. Gao, P. R. Berger, R. G. Hunsperger, G. Zydzik, W. W. Rhodes, H. M. Obryan, D. Sivco, A. Y. Cho, *Appl. Phys. Lett.* **1995**, *66*, 3471.
[28] J. S. Jang, S. J. Park, T. Y. Seong, *J. Vac. Sci. Techno. B* **1999**, *17*, 2667.
[29] V. Aubry, F. Meyer, *J. Appl. Phys.* **1994**, *76*, 7973.

Received: September 24, 2011
Revised: January 2, 2012
Published online: March 5, 2012

